Pergamon

Int. J. Heat Mass Transfer. Vol. 39, No. 9, pp. 1899–1909, 1996

0017-9310/96 $15.00+0.00

0017-9310(95)00270-7

Estimation of the maximum heat flux in the inverted meniscus type evaporator of a flat miniature heat pipe†

D. KHRUSTALEV and A. FAGHRI‡

Department of Mechanical Engineering, University of Connecticut, Storrs, CT 06269-3139, U.S.A.

(*Received* 23 *January* 1995 *and in final form* 10 *July* 1995)

Abstract—A new flat miniature heat pipe configuration for application to cooling electronic components is proposed for high heat fluxes (over 100 W cm^{-2}) on the evaporator wall. The heat pipe contains the inverted meniscus type evaporator and axial capillary grooves covered with a porous plate for the liquid transport. Numerical results for the capillary limit and maximum heat flux, which has been calculated with respect to the formation of the vapor blanket in the porous structure of the evaporator, are presented for a copper–water miniature heat pipe with the external dimensions $2 \times 7 \times 120$ mm.

1. INTRODUCTION

Flat miniature heat pipes with a porous plate and axial grooves for the liquid flow are proposed for the case when only one wall of the evaporator is heated (Fig. 1). The so-called "inverted meniscus scheme" (Raiff and Wayner [1], Feldman and Noreen [2], Solov'ev and Kovalev [3], Wulz and Embacher [4] and Khrustalev and Faghri [5]) is used in the evaporator in order to avoid boiling of the liquid in the liquid channels. This circumstance and also high capillary potential of the porous plate can enable operation of the heat pipe with extremely high heat fluxes, provided that the main constructive parameters are optimized and all of the technological problems have been resolved. For example, the effective pore radius of the copper porous plate, R_p, should be rather small (Freggens [6]), and the porous plate should be sintered with both grooved surfaces under pressure in order to decrease the contact thermal resistance. Because of a significant pressure drop during the vapor flow through miniature channels, the evaporator length should not be large. By the same reason, in both the adiabatic and condenser sections, the fins between vapor channels are deleted in order to provide more space for the vapor flow, as shown in Figs. 1 and 2. The goal of this paper is to estimate the maximum heat flux which can be achieved on the heat pipe evaporator wall before the dry out of the evaporator occurs.

† This work was completed at Wright State University, Dayton, OH 45435, U.S.A.

‡ Author to whom correspondence should be addressed.

2. OPERATION OF THE HEAT PIPE

Since the heat pipe configuration illustrated in Figs. 1 and 2 contains some distinguishing features in comparison with ordinary heat pipes, some explanations concerning the fluid circulation in it are useful for a better understanding of the numerical results. The axial liquid flow takes place along the liquid channels and through the porous plate which is pressed from both sides by the grooved walls of the heat pipe, as shown in Figs. 1 and 2. While heat is added on the evaporator wall, the liquid contained in the wetted porous structure evaporates from the surfaces of the liquid–vapor menisci in the vicinity of the solid fin penetrating the porous plate, Fig. 2(a). The vapor moves through the triangular-shaped channels (in the y-direction) towards the rectangular vapor channels and then along the heat pipe axis (z-coordinate) as can be seen from Fig. 1 where the coordinate system is shown. Since in the condenser section the heat pipe can be cooled from both sides, the condensation of the vapor on the walls of the vapor channel [Fig. 2(b)] takes place on the surfaces of the both porous plate and the heat pipe wall. The condensate forming on the surface of the porous plate is filtered through it mainly into the liquid channels because the pressure in the vapor channel is higher than that in the liquid channels. The condensate forming on the inner surface of the heat pipe wall flows under the influence of the surface tension in a thin film along the y-coordinate towards the corners of the vapor channel, where the bulk liquid resides, and along the z-coordinate (due to the vapor–liquid frictional interaction) toward the condenser end, which is partially blocked with the liquid. The blocking liquid is also filtered through the

NOMENCLATURE

A	cross-sectional area
D_h	hydraulic diameter
f	friction factor coefficient
g	gravity constant
h	heat transfer coefficient
h_{fg}	latent heat of vaporization
$\tilde{K}$	curvature
K	permeability
k_{eff}	thermal conductivity of dry porous structure
k_w	thermal conductivity of solid wall or fin
L	length
L_p	width of the porous plate
N	number of channels
p	pressure
$p_{l\delta}$	bulk liquid pressure near the liquid–vapor interface
$p_{v\delta}$	vapor pressure near the liquid–vapor interface
$\bar{p}_{vb}$	$\int_0^{\delta_{vb}} p_{vb}\mathrm{d}\dot{y}/\delta_{vb}$, mean vapor pressure for a given $\dot{x}$
p_d	disjoining pressure
Q	total heat flow rate
q	heat flux
R_{men}	radius of curvature of the meniscus
$R_{men,o}$	driving meniscus radius (at the surface of the porous plate in the evaporator)
R_p	pore radius
Re	$\bar{w}D_h/\nu$, Reynolds number
T	temperature
t_g	depth of a groove
t_p	total thickness of the porous plate
t_{pen}	depth of the fin penetration into the porous plate
t_w	thickness of the solid wall [Fig. 1(c)]
u_v	area-averaged vapor velocity along the $\dot{x}$ coordinate
$\bar{u}_v$	$\int_0^{\delta_{vb}} u_v\mathrm{d}\dot{y}/\delta_{vb}$, mean vapor velocity along the $\dot{x}$ coordinate for a given $\dot{x}$
v_v	area-averaged vapor velocity along the $\dot{y}$ coordinate
$v_{v\delta}$	vapor blowing velocity (normal to the liquid–vapor boundary)
$\bar{w}$	area-averaged fluid velocity along a channel
W	half-width of a groove
x,y,z	cordinates (Fig. 2)
$\dot{x},\dot{y}$	coordinates (Fig. 3).

Greek symbols

γ	half-angle of the triangular groove
δ_{vb}	thickness of the vapor blanket
δ	thickness of the vapor blanket at the fin top
δ_l	thickness of the thin liquid evaporating film
δ_{max}	maximum thickness of the vapor blanket along the fin surface
ε	$\cos[\arctan(\mathrm{d}\delta_{vb}/\mathrm{d}\dot{x})]$
ϕ	inclination angle from horizontal
φ	porosity
θ_{men}	meniscus contact angle
$\theta_{men,min}$	minimum wetting contact angle
μ	dynamic viscosity
ν	kinematic viscosity
ρ	density
σ	surface tension.

Subscripts

abs	absolute
cap	capillary
ch	channel
e	evaporator
ent	enthalpy
ex	external
eff	effective
l	liquid
ft	filtration
loc	local
men	meniscus
min	minimum
max	maximum
o	outlet
pen	penetration
p	pore
s	solid–liquid interface
sat	saturation
t	total
v	vapor
vb	vapor blanket
w	wall
δ	liquid film free surface.

porous plate under the influence of the pressure drop between the vapor and the liquid channels. The fluid circulation is initiated by the capillary pressure, and the maximum heat transfer capacity of the heat pipe with small heat fluxes on the evaporator wall is usually restricted by the traditional capillary limit (Faghri [7]).

With extremely high heat fluxes, a vapor blanket appears inside the uniform porous structure in the evaporator along the heated solid surface (Raiff and Wayner [1], Solov'yev and Kovalev [3], Wulz and Embacher [4], Khrustalev and Faghri [5]), as shown in Figs. 2(a) and 3(b). In this case, evaporation takes place into the dry region of the porous structure at

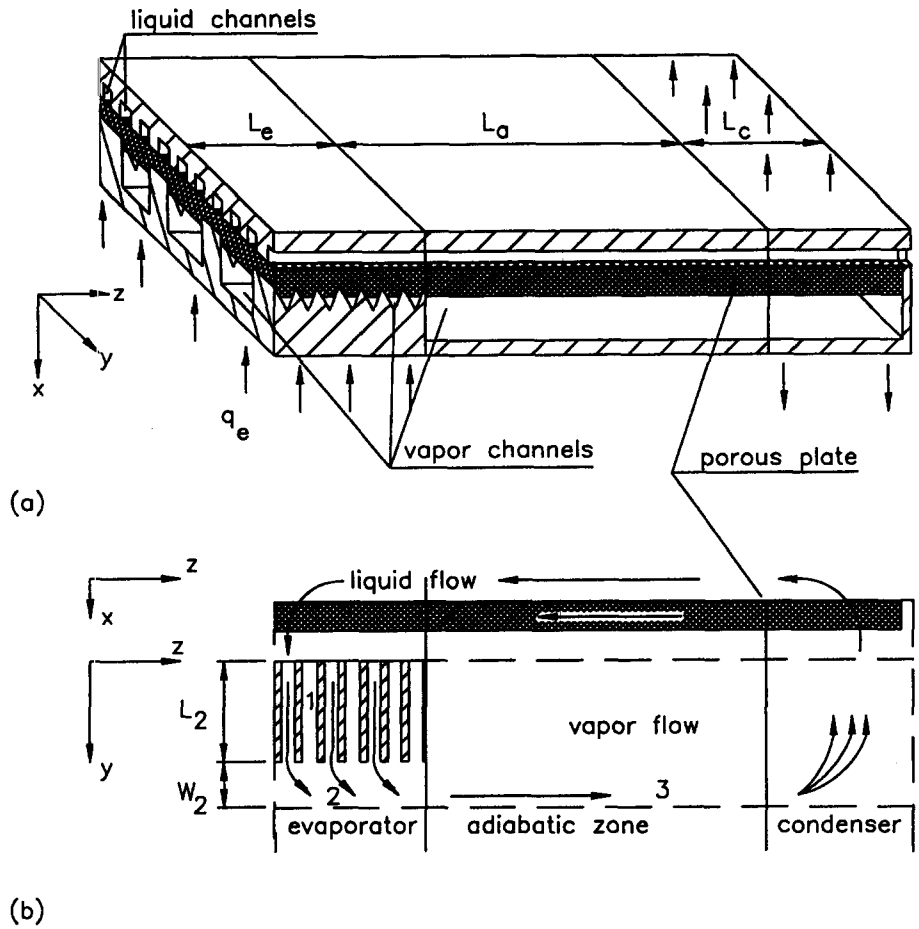

Fig. 1. Flat miniature heat pipe with the inverted meniscus evaporator: (a) schematic of the heat pipe; (b) schematic of the fluid circulation in a characteristic element.

the liquid–vapor interface, the location of which shifts depending on the operational conditions. The heat is conducted to this interface from the heated surface through the dry region of the porous element, and the vapor flows mainly along the solid surface through this dry porous region towards the triangular vapor channel. The vapor flow is provided by the capillary pressure gradient due to the difference in the curvature of the menisci along the liquid–vapor interface inside the porous structure. Therefore, with high heat fluxes, part of the capillary pressure is spent on the compensation of the pressure drop in the vapor flow through the dry porous region. Hence, the maximum heat flux for this configuration should be calculated with respect to the formation of this vapor blanket and can be less than that estimated from the traditional capillary limit. This statement is explained and illustrated with the numerical results in the following sections.

3. CAPILLARY LIMIT FOR THE CASE OF SMALL HEAT FLUXES

Because of the complicated configuration of the heat pipe in the consideration (Figs. 1 and 2), the capillary limit is estimated using the traditional simplified one-dimensional integral approach (Faghri [7]). According to this approach, a balance between the pressure drops in the fluid along the circulation path [Fig. 1(b)] takes place in a heat pipe. For the considered heat pipe this results in the following equation

$$\Delta p_{v,1}+\Delta p_{v,2}+\Delta p_{v,3}+\Delta p_l+\Delta p_{ft,e}+\Delta p_{ft,c}+\Delta p_g=\Delta p_{cap,max}. \quad (1)$$

All of the terms in equation (1) are considered below in detail. For the vapor flow along a heat pipe, it can be assumed that the inertia effects are mutually compensated in the evaporator and condenser sections where acceleration and deceleration of the vapor occur (Dunn and Reay [8]). For the liquid flow the inertia effects are negligible in comparison to those due to viscous losses (Khrustalev and Faghri [9]). The local hydraulic resistances for the vapor flow are also negligible. To estimate the pressure drops due to friction in the channels with fluid flow, the following traditional equation is used:

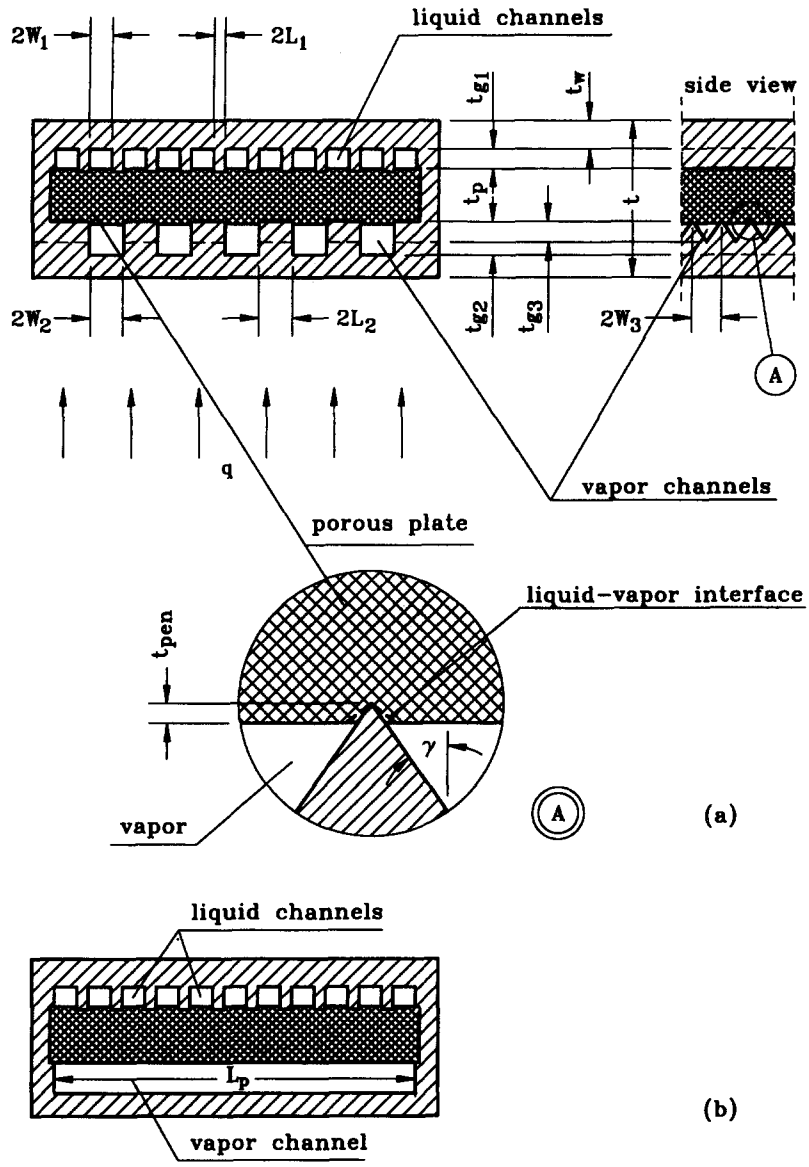

Fig. 2. Cross-sections of the minature heat pipe: (a) evaporator; (b) adiabatic and condenser zones.

$$\Delta p_{v,i} = 2L_{\text{eff},i}\frac{\rho_v \bar{w}_{v,i}^2 f_{v,i}}{D_{h,v,i}} \tag{2}$$

where

$$f_{v,i} = \frac{(fRe)_{v,i}}{Re_{v,i}} = \frac{(fRe)_{v,i}\nu_v}{\bar{w}_{v,i}D_{h,v,i}} \tag{3}$$

$$\bar{w}_{v,i} = \frac{Q_i}{h_{fg}\rho_v A_{v,i}}. \tag{4}$$

The subscript "i" is needed because there are three types of vapor channels in the heat pipe, as shown in Fig. 1: triangular, rectangular (in the evaporator) and flat (in the adiabatic and condenser sections). For these channels $i = 1$, 2 and 3, respectively. $Q_i = Q/N_i$ is the total heat input corresponding to one particular channel with the cross-sectional area $A_{v,i}$. The number of the i-type channels is denoted as N_i, and the total heat load of the heat pipe is Q. Substituting equations (3) and (4) into equation (2), gives

$$\Delta p_{v,i} = 2\frac{(fRe)_{v,i}\mu_v}{\rho_v h_{fg}} Q \frac{L_{\text{eff},i}}{N_i D_{h,v,i}^2 A_{v,i}}. \tag{5}$$

The difference between $\Delta p_{v,i}$ is due to the number and geometry of the channels: N_i, $D_{h,v,i}$, $A_{v,i}$, $L_{\text{eff},i}$ and $(fRe)_{v,i}$. These parameters are specified below for the three types of the vapor channels and also for the liquid channels.

$\Delta p_{v,1}$ in equation (1) is the pressure drop in the short triangular channels in the evaporator along the y-coordinate which is transverse to the axial z-coordinate.

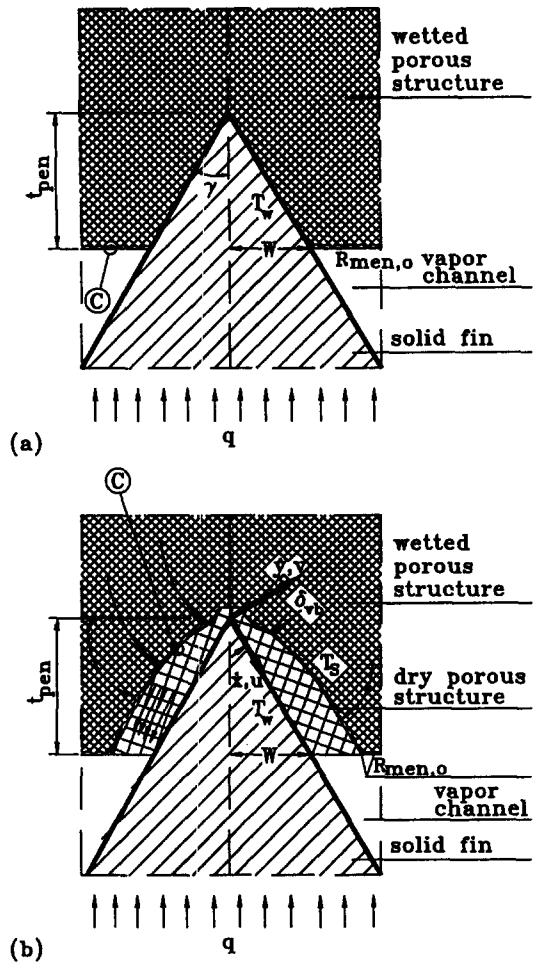

Fig. 3. Schematic of the modeled element of the inverted meniscus type evaporator with the triangular fin: (a) with low heat fluxes; (b) with high heat fluxes.

$$L_{eff,1} = L_2/2 \quad W_3 = t_{g3}/\tan\gamma$$

$$A_{v,1} = (W_3 - t_{pen}\tan\gamma)(t_{g3} - t_{pen})$$

$$D_{h,v,1} = \frac{4(W_3 - t_{pen}\tan\gamma)(t_{g3} - t_{pen})}{2(W_3 - t_{pen}\tan\gamma) + 2(t_{g3} - t_{pen})/\cos\gamma}$$

$$N_{v,1} = L_e L_p/[2W_3(W_2 - L_2)]$$

and $(fRe)_{v,1} = 13.33$ for $\gamma = 30°$ (Shah and Bhatti [10]).

$\Delta p_{v,2}$ is the pressure drop in the rectangular channels in the evaporator where the vapor flows along the z-coordinate (Fig. 2).

$$L_{eff,2} = L_e/2 \quad A_{v,2} = 2W_2(t_{g2} - t_{pen})$$

$$D_{h,v,2} = \frac{4W_2(t_{g2} - t_{pen})}{2W_2 + (t_{g2} - t_{pen})}$$

$$N_{v,2} = 0.5L_p/(W_2 + L_2).$$

For rectangular and flat configurations of a vapor channel, the values of $(fRe)_{v,i}$ can be defined using the following equation (Shah and Bhatti [10]):

$$(fRe)_{v,i} = 24(1 - 1.3553C_i + 1.9467C_i^2 - 1.7012C_i^3 + 0.9564C_i^4 - 0.2537C_i^5) \quad (6)$$

where $C_2 = 0.5(t_{g2} - t_{pen})/W_2$ and the Reynolds number is based on the hydraulic diameter.

$\Delta p_{v,3}$ is the pressure drop in the flat vapor channel in the adiabatic and condenser sections where the vapor flows along the z-coordinate (Figs. 2 and 3).

$$L_{eff,3} = L_a + L_c/2 \quad A_{v,3} = L_p(t_{g2} - t_{pen})$$

$$D_{h,v,3} = \frac{2L_p(t_{g2} - t_{pen})}{L_p + (t_{g2} - t_{pen})} \quad N_{v,3} = 1$$

and $(fRe)_{v,3}$ is also defined from equation (6) where $C_3 = (t_{g2} - t_{pen})/L_p$.

For turbulent flow in a channel when

$$Re_{v,i} = \frac{QD_{h,v,i}}{N_{v,i}h_{fg}\rho_v A_{v,i}\nu_v} > 2300 \quad (7)$$

the following expression is used for $(fRe)_{v,i}$:

$$(fRe)_{v,i} = 0.079Re_{v,i}^{0.75}. \quad (8)$$

The pressure drop during the co-current flow of the liquid in the liquid channels and porous plate, Δp_l, can be estimated as shown below. For the liquid flow in a channel

$$\frac{dp_l}{dz} = \frac{2(fRe)_l\mu_l\bar{w}_{l,ch}}{D_{h,l}^2}. \quad (9)$$

For these channels

$$L_{eff,l} = L_a + (L_e + L_c)/2 \quad A_l = 2W_l t_{gl}$$

$$D_{h,l} = \frac{4W_l t_{gl}}{2W_l + t_{gl}} \quad N_l = 0.5L_p/(W_l + L_l)$$

and $(fRe)_l$ is defined from equation (6) where $C_l = 2W_l/t_{gl}$. For the liquid flow in the porous plate

$$\frac{dp_l}{dz} = \frac{\mu_l\bar{w}_{l,p}}{K}. \quad (10)$$

For any point on z in the adiabatic section the liquid pressure gradients along the z-coordinate in the porous plate and in the liquid channel [equations (9) and (10)] are equal, and they can be assumed to be approximately equal to the entire effective heat pipe length. In a steady-state situation, conservation of mass across any cross section of the heat pipe requires:

$$\frac{Q}{N_l h_{fg}} = \rho_l[2\bar{w}_{l,ch}W_l t_{gl} + 2\bar{w}_{l,p}t_p(W_l + L_l)]. \quad (11)$$

From equations (10) and (11) it follows that

$$\bar{w}_{l,ch} = \frac{Q}{2N_l h_{fg}\rho_l W_l t_{gl}} - \frac{dp_l}{dz}\frac{Kt_p(W_l + L_l)}{\mu_l W_l t_{gl}}. \quad (12)$$

Then, substituting equation (12) into equation (9), the liquid pressure gradient during the co-current liquid flow in the channels and porous plate is

$$\frac{dp_l}{dz} = \left[1 + \frac{2(fRe)_l K t_p (W_l + L_l)}{D_{h,l}^2 W_l t_{gl}}\right]^{-1} \frac{Q(fRe)_l \mu_l}{N_l h_{fg} \rho_l W_l t_{gl} D_{h,l}^2} \quad (13)$$

and the pressure drop in the liquid, with respect to equation (13), is

$$\Delta p_l = \frac{dp_l}{dz} L_{eff,l} = \frac{dp_l}{dz}\left(L_a + \frac{L_e + L_c}{2}\right). \quad (14)$$

Δp_{ft} is the transverse pressure drop due to the filtration of the liquid through the porous plate in the evaporator and condenser sections. Using Darcy's law for this pressure drop we have:

$$\Delta p_{ft,e} = \frac{\mu_l Q t_p}{K h_{fg} \rho_l L_p L_e} \frac{W_l + L_l}{W_l} \quad (15)$$

$$\Delta p_{ft,c} = \frac{\mu_l Q t_p}{K h_{fg} \rho_l L_p L_c} \frac{W_l + L_l}{W_l}. \quad (16)$$

For the case of operation against the gravity field with an inclination angle ϕ, the so-called 'dry' and 'wet' points are usually situated at the end caps of the heat pipe (Faghri [7]). Therefore,

$$\Delta p_g = \rho_l g (L_e + L_c + L_a) \sin \phi. \quad (17)$$

The capillary limit, Q_{cap}, is calculated from equations (1)–(17) and the following condition, which is correct for the case when $R_{men,max} \to \infty$

$$\Delta p_{cap,max} = \frac{2\sigma \cos \theta_{men,min}}{R_p}. \quad (18)$$

4. MAXIMUM HEAT TRANSFER CAPACITY FOR THE CASE OF HIGH HEAT FLUXES

The distinguishing feature of the heat pipe in the consideration is its capability to withstand high heat fluxes on the evaporator wall. For the case of extremely high heat fluxes, a dry zone (vapor blanket) appears in the porous structure along the heated solid surface [Fig. 3(b)]. The vapor flow in the vapor blanket towards the vapor channel takes place with a corresponding pressure drop, Δp_{vb}. The thickness of the vapor blanket, $\delta_{vb}(\dot{x})$, can be calculated using the methodology by Khrustalev and Faghri [5]. The capillary pressure drop $2\sigma/R_{men,o}$, supports the fluid circulation in the heat pipe, described in the following section, while the capillary pressure drop

$$\Delta p_{vb} = 2\sigma(\cos \theta_{men,min}/R_p - 1/R_{men,o}) \quad (19)$$

is expended to compensate for the pressure drop in the vapor flow through the dry porous region. $R_{men,o}$ is the radius of the liquid–vapor meniscus at the outlet of the vapor blanket into the vapor channel or, in other words, the driving meniscus radius at the surface of the porous plate in the evaporator. Since this pressure drop, Δp_{vb}, should be also compensated by the capillary pressure, for the case of high heat fluxes in the evaporator, the pressure balance equation (1) should be rewritten as follows

$$\Delta p_{v,1} + \Delta p_{v,2} + \Delta p_{v,3} + \Delta p_l + \Delta p_{ft,e} + \Delta p_{ft,c} + \Delta p_g = \frac{2\sigma}{R_{men,o}}. \quad (20)$$

It should be also noted that in the considered heat pipe, dry out can take place in the evaporator due to the penetration of the vapor into the liquid channels through the porous plate and the consequent obstruction of the fluid circulation. It can happen when the thickness of the vapor blanket at the top of the fin, δ, is approximately equal to the minimum thickness of the porous plate, $t_p - t_{pen}$. Therefore, in order to determine the effective maximum heat transfer capacity of the heat pipe, Q_{max}, equation (20) should be solved for $R_{men,o}$ with different Q simultaneously with the procedure developed by Khrustalev and Faghri [5] to find δ at the top of the solid heated fin. In the steady-state situation, these two problems (axial fluid circulation and formation of the vapor blanket) have to be solved with the same driving meniscus radius, $R_{men,o}$, and with the condition

$$q_{ex} = \frac{Q}{L_e L_p}. \quad (21)$$

The largest Q at which these two problems can be solved simultaneously is the effective maximum heat transfer capacity of the heat pipe, Q_{max}. The value of Q_{max} for the given operational conditions (which is less than Q_{cap}) can be restricted by either of the two following conditions:

$$\delta = t_p - t_{pen} \quad (22)$$

$$\bar{p}_{vb} - p_{l\delta} \to 0. \quad (23)$$

The first condition, equation (22), corresponds to the penetration of the vapor into the liquid channels. The second condition, equation (23), describes the limiting case when the available capillary potential at the end of the vapor blanket is spent entirely on the vapor flow across the vapor blanket, and therefore, the larger heat fluxes can not be obtained with the same or larger vapor blanket thickness at the fin top, δ. Thus, for the case of the thick porous plate ($t_p - t_{pen} \gg t_{pen}$), Q_{max} is also less than Q_{cap} because, although in this case the thickness of the vapor blanket can be comparatively large, the pressure drop across it can also be comparatively large.

Some explanations should be also given here about the utilized methodology by Khrustalev and Faghri [5] concerning formation of the vapor blanket in the porous structure with high heat fluxes. The model includes the following interconnected problems which are treated simultaneously in the frames of the numerical analysis:

(1) Heat transfer during evaporation from a pore.
(2) Heat transfer and vapor flow in the dry region

of a porous structure with a side boundary, the location of which depends on the operational conditions.

(3) heat conduction in a solid fin with a non-uniform heat sink on the side surfaces.

Only some distinguishing features of this model and several governing equations are represented here for a better understanding of the processes which take place in the evaporator and the numerical results of the present paper. During the evaporation from a pore, the temperature of the free thin liquid film surface, T_δ, is affected by the disjoining and capillary pressures, and also depends on the value of the interfacial resistance, which is defined for the case of a comparatively small heat flux at the interface, q_δ, by the following relation for the heat flux at the interface (Faghri [7]).

$$q_\delta = -\left(\frac{2\alpha}{2-\alpha}\right)\frac{h_{fg}}{\sqrt{(2\pi R_g)}}\left[\frac{p_{v\delta}}{\sqrt{T_v}} - \frac{(p_{sat})_\delta}{\sqrt{T_\delta}}\right] \quad (24)$$

where $p_{v\delta}$ and $(p_{sat})_\delta$ are the saturation pressures corresponding to T_v and at the thin liquid film interface, respectively. The relation between the saturation vapor pressure over the thin evaporating film, $(p_{sat})_\delta$, affected by the disjoining pressure, p_d, and the normal saturation pressure corresponding to T_δ, $p_{sat}(T_\delta)$, is given by the extended Kelvin equation:

$$(p_{sat})_\delta = p_{sat}(T_\delta)\exp\left[\frac{(p_{sat})_\delta - p_{sat}(T_\delta) + p_d - \sigma\tilde{K}}{\rho_l R_g T_\delta}\right]. \quad (25)$$

Equation (25) reflects the fact that under the influence of the disjoining and capillary pressure, the liquid free surface saturation pressure, $(p_{sat})_\delta$, is different from the normal saturation pressure, $p_{sat}(T_\delta)$, and varies along the thin film as well as the temperature of the liquid–vapor interface (Khrustalev and Faghri [11]). For water, the following equation for the disjoining pressure was used in the present analysis (Holm and Goplen [12]):

$$p_d = \rho_l R_g T_\delta \ln\left[a\left(\frac{\delta_l}{3.3}\right)^b\right] \quad (26)$$

where $a = 1.5336$ and $b = 0.0243$. Then, the local heat transfer coefficient during evaporation from the porous surface is defined as

$$h_{e,p} = \frac{\varphi_s}{\pi R_p^2 (T_s - T_v)}\int\int_{A_p} q_\delta \, dA \quad (27)$$

where $\varphi_s \equiv A_p/A_t$ is the surface porosity, which is the ratio of the surface of the pores to the total surface of the porous structure for a given cross-section (in this paper it is assumed that $\varphi_s = \varphi$). Note that the disjoining pressure affects the local evaporative heat transfer coefficient, $h_{e,p}$, as follows from equations (24)–(27).

The heat conduction in the triangular metallic fin is described by the following equation [Fig. 3(b)], which was obtained as a result of an energy balance over a differential element:

$$\frac{d^2 T_w}{d\dot{x}^2} + \frac{dT_w}{d\dot{x}}\frac{1}{\dot{x}} + (T_s - T_w)\frac{k_{eff}\cos\gamma}{\dot{x}\delta_{vb}(\dot{x})k_w \sin\gamma} = 0 \quad (28)$$

where T_s is the local temperature of the porous structure at the liquid–vapor interface location. The local heat flux due to heat conduction across the dry region of the porous structure from the solid surface to the liquid–vapor interface where evaporation takes place is

$$q_{loc}(\dot{x}) = k_{eff}\frac{T_w(\dot{x}) - T_s(\dot{x})}{\delta_{vb}(\dot{x})}. \quad (29)$$

Equation (29) is valid for the case $k_v \ll k_{eff}$ and $c_{p,v}(T_w - T_s) \ll h_{fg}$. Hence, the mean velocity of the vapor flow for a given $\dot{x}$ along the solid surface is (using the mass and energy conservation balances):

$$\bar{u}_v(\dot{x}) = \frac{1}{\delta_{vb}(\dot{x})h_{fg}\rho_v}\int_0^{\dot{x}} q_{loc}(\dot{x})\, d\dot{x} \equiv \frac{k_{eff}}{\delta_{vb}(\dot{x})h_{fg}\rho_v}\int_0^{\dot{x}} \frac{T_w(\dot{x}) - T_s(\dot{x})}{\delta_{vb}(\dot{x})} d\dot{x} \quad (30)$$

where $\bar{u}_v(\dot{x})$ is the mean vapor velocity along the $\dot{x}$-coordinate. The modified Darcy's equations for the vapor flow in both directions through a porous structure where the value of 0.55 is used for a dimensionless form-drag constant (Nield and Bejan [13]) are

$$\frac{\partial p_{vb}}{\partial \dot{x}} = -\frac{\mu_v}{K}u_v(\dot{x}) - \frac{0.55}{\sqrt{K}}\rho_v u_v^2(\dot{x}) \quad (31)$$

$$\frac{\partial p_{vb}}{\partial \dot{y}} = \frac{\mu_v}{K}v_v(\dot{y}) + \frac{0.55}{\sqrt{K}}\rho_v v_v^2(\dot{y}) \quad (32)$$

where u_v and v_v are the area-averaged vapor velocities. Now, the equation for T_s should be derived. The local heat flux at the liquid–vapor interface due to the evaporation of the liquid is:

$$q_{loc}(\dot{x}) = [T_s(\dot{x}) - T_v(\dot{x})]h_{e,p}(\dot{x}). \quad (33)$$

Combining equations (29) and (33) because of the steady-state situation in the consideration, the expression for the local temperature of the porous structure at the liquid–vapor interface location is:

$$T_s(\dot{x}) = \frac{T_w(\dot{x}) + h_{e,p}(\dot{x})T_v(\dot{x})\delta_{vb}(\dot{x})/k_{eff}}{1 + h_{e,p}(\dot{x})\delta_{vb}(\dot{x})/k_{eff}}. \quad (34)$$

It is anticipated that the liquid–vapor interface can be stable provided it has the shape which eliminates the influence of the inertia effects due to acceleration of the vapor flow on the vapor pressure near this interface. While the steady-state situation is analyzed, the liquid pressure along the interface is constant, and

Table 1. Geometrical characteristics of the miniature heat pipe

W_1	W_2	W_3	t_{g1}	t_{g2}	t_{g3}	L_e	L_a	L_c
0.1 mm	0.3 mm	0.23 mm	0.3 mm	0.7 mm	0.4 mm	10 mm	90 mm	20 mm
L_p	L_1	L_2	t_w	t_p	t_{pen}	R_p	K	γ
6 mm	0.1 mm	0.3 mm	0.3 mm	0.6 mm	0.2 mm	0.02 mm	1×10^{-12} m^2	30°

the pressure losses in the vapor flow in both directions due to friction and solid obstacles are compensated by the capillary pressure, the vapor pressure gradient along the stable interface due to these inertia effects should be equal to zero. Since the velocity profile of the vapor flow along the $\dot{x}$-coordinate is nearly uniform, it means that

$$\frac{\rho_v \bar{u}_v^2}{2} + \frac{\rho_v v_{v\delta}^2 \varepsilon^2}{2} = \text{constant} \tag{35}$$

where $\varepsilon = \cos[\arctan(\mathrm{d}\delta_{vb}/\mathrm{d}\dot{x})]$ is the cosine of the angle between the $\dot{y}$ coordinate and the normal to the liquid–vapor interface, and $v_{v\delta}$ is the blowing velocity (normal to the liquid–vapor interface):

$$v_{v\delta} = k_{eff}\frac{T_w - T_s}{\delta_{vb} h_{fg} \rho_v}. \tag{36}$$

Note that equation (35) is not used for the fluid flow in the porous medium but describes the inertia effects at the adjustable liquid–vapor interface while the momentum equations for the vapor flow in the porous medium are concerned. Equation (35) is necessary in order to find the equilibrium location of the liquid–vapor boundary. Equation (36) implies that the total amount of energy, transferred from the heated solid surface to the liquid–vapor interface by the heat conduction across the dry porous zone, is spent on vaporization of the liquid. Although the vapor leaving the dry zone of the porous structure is superheated, it is convenient to relate the local effective heat transfer coefficient to the vapor saturation temperature because $c_{p,v}(T_w - T_s) \ll h_{fg}$. Thus the local effective heat transfer coefficient corresponding to the point $\dot{x} = L_{vb}$ (outlet of the vapor flow) is defined as:

$$h_{eff,pen} = \frac{1}{W(T_w - T_v)_o}\int_0^{L_{vb}} k_{eff}\frac{T_w(\dot{x}) - T_s(\dot{x})}{\delta_{vb}(\dot{x})}\mathrm{d}\dot{x}. \tag{37}$$

In the numerical results of Khrustalev and Faghri [5], the pressure drop in the vapor blanket along the fin surface with turbulent vapor flow in the pores was many times larger than the estimated pressure drop in the liquid over the porous element. That enabled the assumption of the constant liquid pressure along the liquid–vapor boundary.

5. NUMERICAL TREATMENT, RESULTS AND DISCUSSION

The numerical results were obtained for the case of the miniature heat pipe, the characteristic dimensions of which are listed in Table 1. The working fluid was water, $\theta_{men,min} = 33°$ (Stepanov *et al.* [14]), $\alpha = 0.05$ (Paul [15]), $k_{eff} = 10$ W m^{-1} K^{-1}, $k_w = 379$ W m^{-1} K^{-1}, $\varphi = 0.35$. The calculations were made with constant thermophysical properties corresponding to the operating temperature, T_v. The superheat of the vapor in the dry zone of the porous structure was neglected. Therefore, the maximum heat transfer capacity of the heat pipe was underestimated because the vapor enthalpy heat transfer, $Q_{v,ent}$, was not taken into account. The relative error for $q_{ex,max}$ because of this assumption can be estimated as follows

$$\frac{Q_{v,ent}}{Q} \approx \frac{c_{p,v}}{h_{fg}}\frac{(T_0 - T_v)}{2} \approx \frac{c_{p,v}}{2h_{fg}}\frac{q_{ex}}{h_{eff,ex}} \tag{38}$$

where T_0 is the temperature of the fin top. This error does not exceed 9% for the presented results.

In order to find the effective maximum heat transfer capacity of the heat pipe, Q_{max}, a graphical method was used as explained below. In the first step, the dependence of the driving meniscus radius on heat load, $R_{men,o}(Q)$, resulting from equation (20) was obtained and plotted for a given operating temperature, T_v. In the second step, another dependence $R_{men,o}(Q)$, resulting from the solution of the vapor blanket formation for a given thickness of the vapor blanket at the fin top, δ, was obtained and plotted in the same figure. The intersection of these two curves gives the values of Q and $R_{men,o}(Q)$ which correspond to the steady-state with the chosen δ. Repeating this process with different values of δ, the function $\delta(Q)$ was obtained, and the maximum heat transfer capacity, Q_{max}, for the steady-state was defined with respect to the conditions (22) and (23). In Figs. 4–6 the values of the maximum heat transfer capacity, Q_{max}, found by this method for different operating temperatures, T_v, are indicated by the ring and square symbols for horizontal and vertical (the evaporator end of the heat pipe is elevated) orientations, respectively. The bullets in these figures correspond to the situations when $\delta = t_p - t_{pen}$ and $\bar{p}_{vb} - p_{l,\delta} \to 0$ simultaneously, which determines the absolute maximum heat transfer capacity in the evaporator, $Q_{max,abs}$, which can be reached in some cases as discussed further. For $T_v = 120°C$, $Q_{max} = Q_{max,abs} = 116.4$ W for the horizontal orientation and $Q_{max} = 93$ W for the vertical orientation, as shown in Fig. 4(a). For lower operating temperatures the maximum heat transfer capacity is smaller; for example, for $T_v = 90°C$ at the steady-state $Q_{max} = 26$ W for the horizontal orientation, $Q_{max} = 36$ W for the vertical orientation, and $Q_{max,abs} = 45$ W, as shown in Fig.

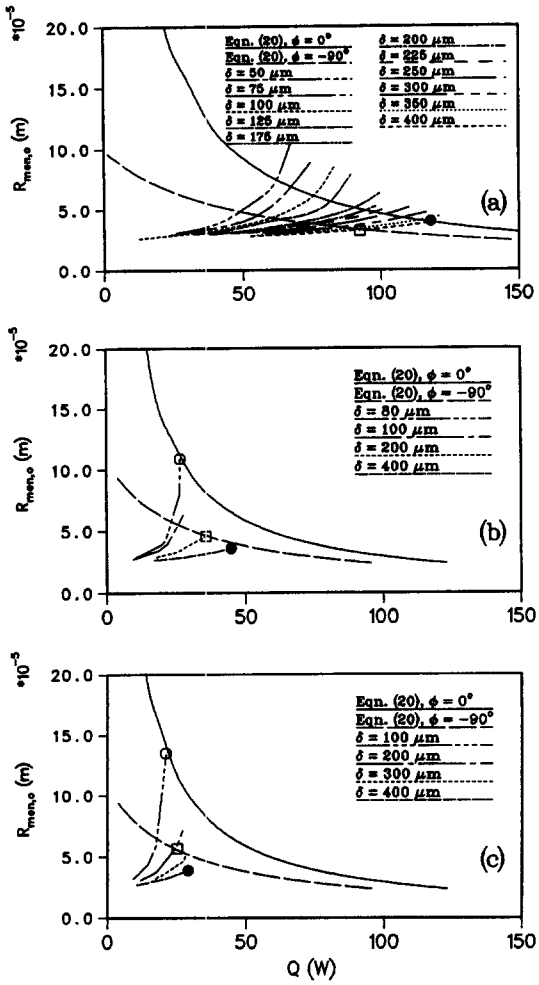

Fig. 4. Variation of the driving meniscus radius and thickness of the vapor blanket at the fin top with heat input: (a) $T_v = 120°C$, $K = 1.0 \times 10^{-12}$ m^2; (b) $T_v = 90°C$, $K = 1.0 \times 10^{-12}$ m^2; (c) $T_v = 90°C$, $K = 0.5 \times 10^{-12}$ m^2.

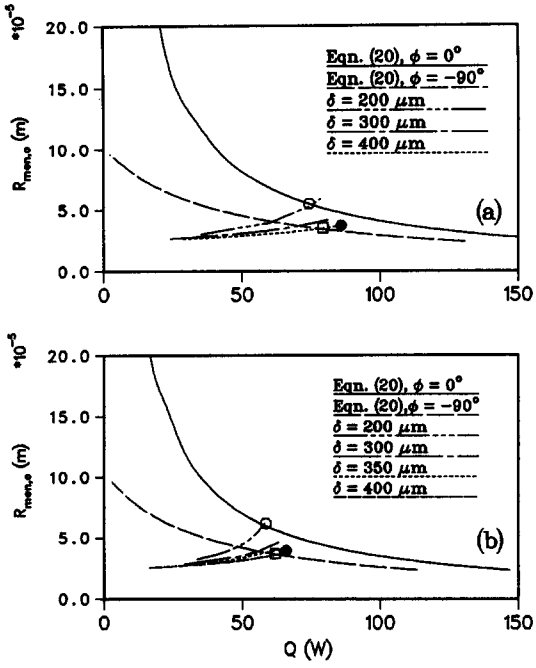

Fig. 5. Variation of the driving meniscus radius and thickness of the vapor blanket at the fin top with heat input ($K = 1.0 \times 10^{-12}$ m^2): (a) $T_v = 110°C$; (b) $T_v = 100°C$.

4(b). While for the heat input of 45 W at $T_v = 90°C$, a steady-state does not exist (within the frames of the considered model), there is no restriction of the heat transfer because of the axial fluid circulation for the heat load lower than 45 W. Therefore, an unstable regime of the heat pipe operation can occur with heat loads from 26 to 45 W for the horizontal orientation and from 36 to 45 W for the vertical orientation at $T_v = 90°C$. Physical models of unstable regimes are not obvious yet. Ku [16] referred to the regime when the vapor bubbles (instead of the vapor blanket) form at the heating surface and migrate until vented into vapor channel. Other models of the unstable regimes are also possible. Comparison of Figs. 4(b) and (c) shows that for a decreased permeability of the porous structure Q_{max} is smaller. It can be also seen from Figs. 4 and 5 that with the growth of the operating temperature Q_{max} increases.

Analyzing Fig. 4(a), once can come to the conclusion that the thickness of the vapor blanket at the fin top, δ, increases with the heat load, which should result in the decrease of the effective heat transfer coefficients and lead to larger temperature drops in the evaporator. These trends are presented in Fig. 6 for the horizontal orientation. Two characteristic temperature drops are shown in Fig. 6(a), both being related to the operating temperature, T_v. The first is measured from the temperature of the external surface of the heat pipe wall, T_{ex}, and the second is the superheat of the solid particles of the porous structure at the liquid–vapor boundary of the vapor blanket over the operating temperature, $T_s - T_v$, at the outlet of the vapor blanket into the vapor channel ($\dot{x} = t_{pen}/\cos\gamma$). The last temperature drop does not increase with the heat flux on the external surface of the evaporator, q_{ex}, because for larger heat fluxes the radii of the menisci along the vapor blanket are smaller, which results in the increase of the local heat transfer coefficients during the evaporation from the pores. That is why $T_s - T_v < 20°C$ even for the enormously high heat fluxes of 200 W cm^{-2}, which means that the evaporative regime is predominant at the boundary of the vapor blanket. However, a mixed regime of vaporization at this boundary when both the evaporation and formation of the small vapor bubbles occur can be imagined without changing the entire physical model. The total temperature drop, $T_{ex} - T_v$, consists of the several components: those in the metallic wall and fin, across the vapor blanket, and that corresponding to the evaporation from the liquid–vapor interface, which can be expressed by the following equation:

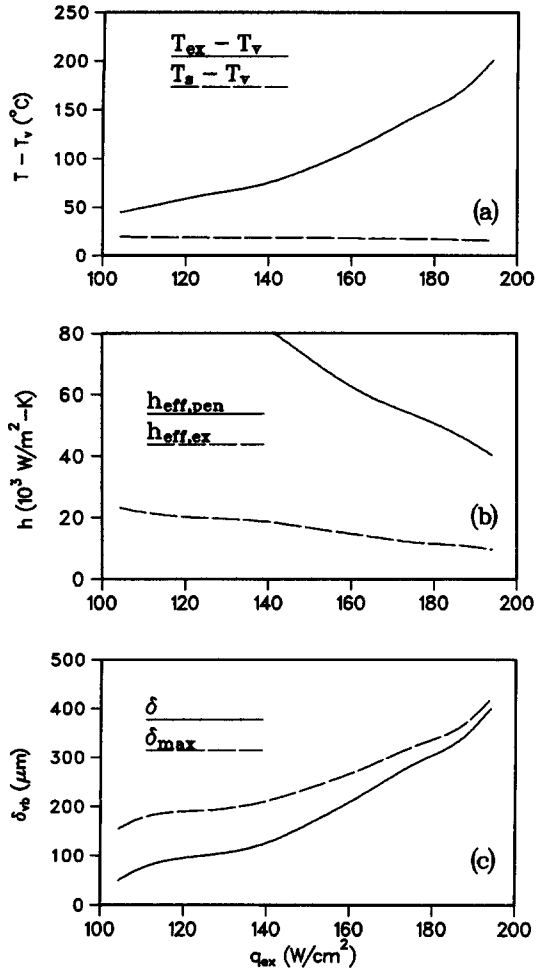

Fig. 6. Performance characteristics of the heat pipe evaporator ($T_v = 120°C$, $K = 1.0 \times 10^{-12}$ m^2, horizontal orientation): (a) temperature drops; (b) heat transfer coefficients; (c) vapor blanket thickness.

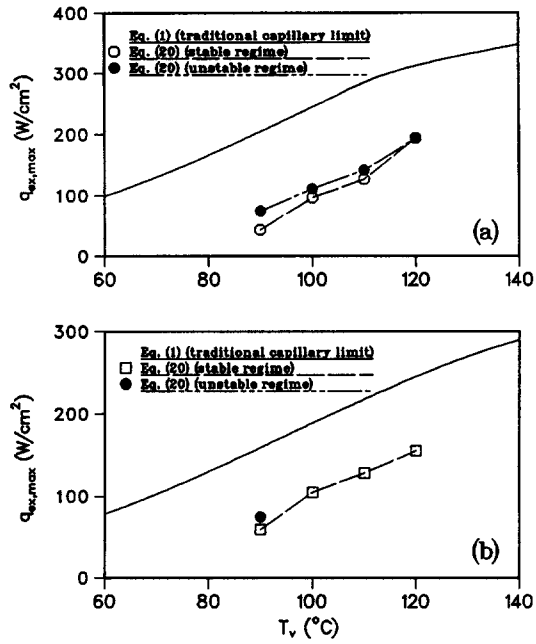

Fig. 7. Dependence of the maximum heat flux in the heat pipe evaporator on the operating temperature ($K = 1.0 \times 10^{-12}$ m^2): (a) horizontal orientation; (b) vertical orientation.

$$\frac{T_{ex}-T_v}{q_{ex}} = \frac{t_w}{k_w} + \frac{W_2+L_2}{L_2}\left[\frac{t_{g2}-t_{g3}}{k_w} + \frac{2L_2}{L_2+t_{pen}\tan\gamma}\frac{t_{g3}-t_{pen}}{k_w} + \frac{1}{h_{eff,pen}}\frac{W_3}{t_{pen}\tan\gamma}\right]. \quad (39)$$

While the temperature drops in the metallic walls of the heat pipe are comparatively small, it can be seen in Fig. 6(a) that the main component of the total temperature drop is that across the dry porous structure zone due to the heat conduction from the fin surface to the liquid–vapor interface. The total temperature drop increases progressively with the heat flux and reaches almost 200°C when q_{ex} approaches 200 W cm^{-2}. This happens because the thickness of the vapor blanket, δ_{vb}, increases and the effective heat transfer coefficients, $h_{eff,pen}$ and $h_{eff,ex}$, decrease with the heat flux as shown in Figs. 6(b) and (c). Therefore, the thermal conductivity of the porous structure plays an important role in the heat transfer in the evaporator. $h_{eff,pen}$ is the effective heat transfer coefficient concerning only the part of the fin penetrating the porous structure [equation (37)], and $h_{eff,ex}$ is the total effective heat transfer coefficient defined as follows:

$$h_{eff,ex} = \frac{q_{ex}}{T_{ex}-T_v}. \quad (40)$$

Two curves in Fig. 6(c) correspond to the minimum and maximum thicknesses of the vapor blanket at the fin top and at the vapor blanket outlet into the vapor channel, respectively. It follows from this figure that when the vapor blanket is comparatively thick, it is almost uniform along the heated surface.

From Figs. 4 and 5, the dependencies of the maximum heat flux, which can be reached on the evaporator wall, on the operating temperature result for the cases of horizontal and vertical orientations, Fig. 7. The maximum heat fluxes, predicted by the model accounting for the vapor blanket formation in the porous structure, are much smaller than those obtained from the traditional capillary limit calculations. The zone situated between the two lower curves in Fig. 7(a) supposedly corresponds to the unstable regime of the heat pipe operation. However, for the temperatures higher than 120°C only the stable regime takes place for all values of the heat flux which can be as high as 200 W cm^{-2}. For operating temperatures lower than 100°C the maximum heat flux does not exceed 100 W cm^{-2}. Figure 7(b) indicates that the heat pipe can successfully operate against the gravity field

6. CONCLUSIONS

The results of the numerical modeling of the miniature copper–water heat pipe with the inverted meniscus type evaporator are summarized as follows:

1. At high heat fluxes part of the available capillary potential is expended on the compensation of the pressure drop in the vapor flow through the dry region of the porous structure in the evaporator. As a result of this, the dry out of the inverted meniscus type evaporator of the heat pipe occurs with the maximum heat flux on the evaporator wall which is about two times smaller than that corresponding to the traditionally calculated capillary limit.

2. The proposed heat pipe configuration with the external dimensions $2 \times 7 \times 120$ mm is capable of withstanding high heat fluxes on the evaporator wall which can be about 200 W cm^{-2} for the horizontal orientation and 150 W cm^{-2} for the vertical orientation at the operating temperature of 120°C.

3. The unstable operating regime can possibly occur in the heat pipe with heat fluxes on the evaporator wall which are close to the maximum, especially for the operating temperatures lower than 100°C.

4. The effective evaporative heat transfer coefficient decreases with the heat flux on the evaporator external wall because of the growth of the vapor blanket thickness inside the porous structure.

5. With high heat fluxes, the temperature drop of the heat pipe evaporator can be critical for the heat pipe applications. The main component of the temperature drop in the evaporator is that across the vapor blanket due to the heat conduction from the heated solid surface to the liquid–vapor interface. Therefore, it is reasonable to chose the porous structure with high thermal conductivity, permeability, and capillary potential.

Acknowledgements—Funding for this work was provided by the National Science Foundation Grant CTS-941458 and Thermal Energy Group of the Aero Propulsion Directorate of the U.S. Air Force under contract no. F33615-92-C-2276.

REFERENCES

1. R. J. Raiff and P. C. Wayner, Jr, Evaporation from a porous flow control element on a porous heat source, *Int. J. Heat Mass Transfer* **16,** 1919–1929 (1973).
2. K. T. Feldman and D. L. Noreen, Design of heat pipe cooled laser mirrors with an inverted meniscus evaporator wick, *Proceedings of the AIAA 18th Aerospace Sciences Meeting*, Pasadena, California, AIAA-80-0148 (1980).
3. S. L. Solov'ev and S. A. Kovalev, Heat transfer and hydrodynamics in the inverted meniscus evaporator of a heat pipe, *Proceedings of the 6th International Heat Pipe Conference*, Grenoble, France, Vol. I, pp. 116–120 (1987).
4. H. Wulz and E. Embacher, Capillary pumped loops for space applications experimental and theoretical studies on the performance of capillary evaporator designs, *Proceedings of the AIAA/ASME 5th Joint Thermophysics and Heat Transfer Conference*, Seattle, WA, AIAA 90-1739 (1990).
5. D. Khrustalev and A. Faghri, Heat transfer in the inverted meniscus type evaporator at high heat fluxes, *Int. J. Heat Mass Transfer* **38,** 3091–3101 (1995).
6. R. A. Freggens, Experimental determination of wick properties for heat pipe applications, *Proceedings of the 4th Intersociety Energy Conversion Conference*, Washington, D.C., pp. 888–897 (1968).
7. A. Faghri, *Heat Pipe Science and Technology*. Taylor & Francis (1995).
8. P. D. Dunn and D. A. Reay, *Heat Pipes* (3rd Edn). Pergamon Press, Oxford (1982).
9. D. Khrustalev and A. Faghri, Thermal analysis of a micro heat pipe, *ASME J. Heat Transfer* **116**(1), 189–198 (1994).
10. R. K. Shah and M. S. Bhatti, Laminar convective heat transfer in ducts. In *Handbook of Single Phase Convective Heat Transfer* (Edited by Kakac *et al.*). John Wiley, New York (1987).
11. D. Khrustalev and A. Faghri, Heat transfer during evaporation and condensation on capillary-grooved structures of heat pipes, *Proceedings of the* 1994 *International Mechanical Engineering Congress*, Chicago, IL., HTD-Vol. 287, pp. 47–59 (1994); also to appear in *ASME J. Heat Transfer*.
12. F. W. Holm and S. P. Goplen, Heat transfer in the meniscus thin-film transition region, *ASME J. Heat Transfer* **101**(3), 543–547 (1979).
13. D. A. Nield and A. Bejan, *Convection in Porous Media*. Springer, New York (1992).
14. V. G. Stepanov, L. D. Volyak, and Yu. V. Tarlakov, Wetting contact angles for some systems, *J. Engng Phys. Thermophys.* **32**(6), 1000–1003 (1977).
15. B. Paul, Compilation of evaporation coefficients, *ARS J.* **32,** 1321–1328 (1962).
16. J. Ku, Overview of capillary pumped loop technology *Proceedings of the 29th National Heat Transfer Conference*, Atlanta, GA (1993).